# Multi-Orbit Spectrum Sensing for Uplink NOMA System Toward Next-Generation IoT Networks

Tianheng Xu, *Member, IEEE*, Yinjun Xu, *Member, IEEE*, Jingyi Wu, Haijun Zhang, *Fellow, IEEE*, Ting Zhou, *Member, IEEE*, Honglin Hu, *Senior Member, IEEE*, and Victor C. M. Leung, *Life Fellow, IEEE*

***Abstract*—Next-generation Internet of Things(IoT) technology is vital for sixth-Generation(6G) communication systems, driving exponential growth in spectrum resource demand. Spectrum sensing, essential for identifying unused spectrum, and Non-Orthogonal Multiple Access(NOMA), which allows efficient frequency band sharing among users, can significantly improve spectrum efficiency. However, current sensing methods do not fully support NOMA, resulting in suboptimal performance. Motivated by such a circumstance, we propose a feature-based spectrum sensing method for uplink communication in power-domain NOMA IoT scenarios with multi-user interference, aiming to maximize both static and dynamic spectrum efficiency. Firstly, we introduce the notion of orbits to represent non-fully occupied spectral holes. Then we elaborate on the sensing criterion as well as workflow and design the two-stage spectrum sensing framework, which proposes the orbit estimation sensing algorithm in the stage 1 and accurate sensing threshold in the stage 2, to mitigate false alarm fluctuations. The closed-form solution for the estimation threshold and accurate threshold configuration are derived thereafter. Simulation results show that our proposed multi-orbit sensing method has stable performance and achieves average 30% system throughput gains compared to the latest NOMA techniques at 5 dB.**

***Index Terms*—Spectrum sensing, next-generation IoT, feature detection, multi-orbit estimation, NOMA.**

Received 20 July 2024; revised 10 December 2024 and 27 March 2025; accepted 25 May 2025. Date of publication 6 June 2025; date of current version 14 November 2025. This work was supported in part by the National Key Research and Development Program of China under Grant 2024YFB2908600, in part by the Science and Technology Commission Foundation of Shanghai under Grant 24DP1500700 and Grant 24DZ2200100, in part by the National Natural Science Foundation of China under Grant U22B2003 and Grant U2441227, in part by Beijing Natural Science Foundation under Grant L241008, and in part by the Fundamental Research Funds for the Central Universities under Grant FRF-TP-22-002C2. An earlier version of this paper was presented at the IEEE ICC 2024 [DOI: 10.1109/ICC51166.2024.10622988]. The associate editor coordinating the review of this article and approving it for publication was B. Shim. *(Corresponding author: Ting Zhou.)*

Tianheng Xu is with Shanghai Advanced Research Institute, Chinese Academy of Sciences, Shanghai 201210, China, and also with Shanghai Frontier Innovation Research Institute, Shanghai 201100, China (e-mail: xuth@sari.ac.cn).

Yinjun Xu is with Shanghai Advanced Research Institute, Chinese Academy of Sciences, Shanghai 201210, China, and also with the School of Electronic, Electrical and Communication Engineering, University of Chinese Academy of Sciences, Beijing 100049, China (e-mail: xuyj@sari.ac.cn).

Jingyi Wu and Honglin Hu are with Shanghai Advanced Research Institute, Chinese Academy of Sciences, Shanghai 201210, China (e-mail: wujy@sari.ac.cn; hlhu@ieee.org).

Haijun Zhang is with the Institute of Artificial Intelligence, Beijing Advanced Innovation Center for Materials Genome Engineering, Beijing Engineering and Technology Research Center for Convergence Networks and Ubiquitous Services, University of Science and Technology Beijing, Beijing 100083, China (e-mail: haijunzhang@ieee.org).

Ting Zhou is with the School of Microelectronics, Shanghai University, Shanghai 201210, China, and also with Shanghai Frontier Innovation Research Institute, Shanghai 201100, China (e-mail: zhouting@shu.edu.cn).

Victor C. M. Leung is with the Artificial Intelligence Research Institute, Shenzhen MSU-BIT University, Shenzhen 518172, China, also with the College of Computer Science and with Software Engineering, Shenzhen University, Shenzhen 518060, China, and also with the Department of Electrical and Computer Engineering, The University of British Columbia, Vancouver, BC V6T 1Z4, Canada (e-mail: vleung@ieee.org).

Digital Object Identifier 10.1109/TWC.2025.3574710

## I. Introduction

PRESENTLY, the fifth Generation (5G) mobile communication systems are commercially available worldwide, while a global consensus has been reached on the vision for the sixth Generation (6G) mobile communication systems. Therefore, the world is currently focusing on researching 5G-Advanced (5G-A) and gradually moving towards 6G [2], [3], [4], [5], [6]. The proliferation of communication devices experienced an exponential surge during the 5G era. Looking ahead to the future of 6G, the number of these devices is expected to substantially increase further. Therefore, the concept of ubiquitous connectivity and the Internet of everything has emerged as a prominent megatrend for the future [7], [8], [9], [10].

One representative belongs to the next-generation of the Internet of Things (IoT) [11], [12], [13], [14], [15]. The traditional IoT concept envisions an upcoming time in which all entities are interconnected through a vast array of physical devices and sensing nodes. On top of this foundation, the next-generation of IoT improves upon mere interconnectivity to cover intelligent connectivity across all entities [16], [17], [18]. Furthermore, it broadens the scope from terrestrial IoT to include an integrated IoT that spans the whole physical realm in a wide-area, three-dimensional, and ubiquitous-connectivity manner, involving numerous network components, such as diverse terrestrial cellular terminals, data centers, intelligent cars, uncrewed aerial vehicles, high altitude platforms and satellite Internet etc. [19], [20], [21]. This development ensures that IoT devices have superior communication capabilities, distinguished by intelligence and efficiency, resulting in improved energy efficiency and reduced latency.

However, high technical indices also introduce new problems and challenges. Present IoT technologies cannot well satisfy the demanding quality standards of 6G regarding IoT quality of service. For instance, the connectivity density has risen from $10^6$ to $10^7$ devices/km$^2$ and in a 6G-based intelligent network, all types of communication terminals and

mobile devices should have the ability of artificial intelligence simultaneously [22], [23]. Currently, due to the high connectivity density, the scarcity of spectrum resources is further exacerbated. Challenges like these present a huge obstacle to the development of the next-generation IoT.

Spectrum sensing technology has been proposed as a solution to the problem of spectrum scarcity in wireless communication systems, which allows unauthorized users to use the licensed frequency band for communication by detecting spectral holes in the surrounding radio environment [24], [25], [26], [27], [28]. Meanwhile, dynamic resource allocation can effectively manage available resources, which provides better utilization rates compared to fixed resource allocation. Both of them can bring "Stock Enhancement", thus, using these two technologies to maximize the utilization of free spectrum resources is a hot research topic in ubiquitous IoT scenarios. In [29], Surekha and Rahman developed a model that integrates game theory with spectrum sensing to analyze the spectrum efficiency of IoT networks based on cognitive radio technology. Reference [30] combined with blockchain and proposed a trust-centric privacy-preserving blockchain for dynamic spectrum access in IoT networks. While in [31], a novel intrusion detection system was specifically designed for IoT spectrum sensors using host-based and federated learning approaches. Reference [32] proposed an effective scheduling method for radio resources using the current dynamic resource block structure, obtaining strong data rates, system throughput, and spectral efficiency. In [33], He et al. enabled fast-adaptive resource allocation for dynamic vehicular environments through meta-hierarchical reinforcement learning.

On the other hand, compared with the widely used Orthogonal Multiple Access (OMA) technology, NOMA is a static and periodic technology, which can be applied to improve the spectrum utilization and increase the system capacity effectively [34], [35]. NOMA has shown significant enhancements within the massive IoT network. For instance, power-domain NOMA allocates different users in the same block of time-frequency resources based on their powers, which is then decoded through the successive interference cancellation technique [36], [37]. In contrast to the conventional dynamic usage of spectrum resources with spectrum sensing, NOMA expands resources to reinforce the upper bound of spectrum resource utilization, resulting in an "incremental effect". Recently, some works in the literature were contributed for NOMA in IoT networks [38], [39], [40], [41], [42], [43], [44].

In [38], Pavan and Harigovindan proposed a power-optimized NOMA with transmission opportunity tuning for IEEE 802.11ah dense IoT networks. Reference [39] presented an energy-efficient alternating optimization framework based on cooperative NOMA for next-generation IoT-enabled communication networks and exploited a zero-forcing-based active-beamforming technique at the source node. In [40], an IoT framework based on downlink NOMA-hybrid automatic repeat request was proposed, utilizing intelligent reflecting surfaces to enhance the performance of IoT devices in non-line-of-sight regions. In [41], Wang et al. suggested implementing both the mixed block strategy and uniform block strategy to enhance the system performance of a NOMA-enabled IoT uplink network with varying types of devices. Reference [42] introduced dual uncrewed aerial vehicles to aid in the auxiliary communication for IoT networks in NOMA scenarios while minimizing energy consumption to enhance IoT network capacity. For cooperative NOMA, [43] proposed a simultaneous wireless information and power transfer IoT networks, where an energy-harvesting approach provides services to two IoT users via multiple energy-limited relay nodes. Finally, in [44], focusing on the IoT-satellite terrestrial relay network scenario, Tubiana et al. designed a random access protocol based on Q-learning for massive access devices to improve network performance.

There is no inherent conflict between the combination of spectrum sensing along with dynamic resource allocation and NOMA. By integrating these technologies, "incremental effect" and "stock enhancement" of spectrum resources can be simultaneously obtained, creating an opportunity for open-source and cost-effective ubiquitous IoT implementation. However, the combination of NOMA-level spectrum sensing and dynamic resource allocation has introduced new challenges and problems. For instance, the NOMA system faces multi-user sensing interference problems where the sensing quality of secondary users gets worse as the number of users increases. Moreover, the randomness of resource allocation by users in the NOMA system exacerbates interference complexities, leading to a significant challenge in accurately sensing the secondary users. Motivated by such a circumstance, in this paper, we focus on the dynamic spectrum sensing and resource utilization for the uplink power-domain NOMA system towards next-generation IoT networks. Our preliminary study in [1] presented an initial concept of the orbit-based spectrum sensing. In the light of our previous work, this research carries out an enhanced technique, i.e. multi-orbit spectrum sensing method. The novel contributions of this research can be summarized as follows.

- Firstly, we elaborate the criteria and workflow of the multi-user spectrum sensing technology for the uplink power-domain NOMA IoT system, which can identify the transmission status of non-orthogonal overlapped users and exploit the detected non-fully occupied spectral holes.
- Secondly, we investigate the fluctuation phenomenon of false-alarm probability and analyze the underlying reasons. The random and independent transmission willingness of each primary user is a major cause of this phenomenon. Subsequently, we propose a two-stage sensing method, which contains orbit estimation in the stage 1 and accurate sensing in the stage 2, to enhance fault tolerance and mitigate the aforementioned false-alarm probability fluctuation.
- Thirdly, we deduce the closed-form solution for the estimation threshold and accurate sensing threshold in the typical 3-user NOMA systems and expand to $N$-user scenarios, which based on the impact of the transmitting uncertainty and the overlapping as well as provides a theoretical basis for optimizing parameters in practical application.
- Finally, we confirm the effectiveness of the proposed method through simulation experiments. Numerical

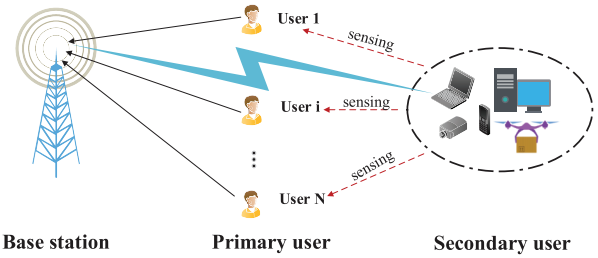


Fig. 1. System model.

results manifest that the complete version of proposed method not only enhances detection performance for user overlapping scenarios, but also successfully suppresses the issue of false alarm fluctuation. Compared to the latest related NOMA technologies, it obtains an average of 30% system throughput gains, which emphasizes the potential benefits of implementing in practice.

The paper is structured as follows. Section II provides a brief presentation of the system model and the spectrum sensing preprocessing. The basic workflow, the derivation of the false alarm probability, and the proposed multi-orbit sensing method are detailed in Section III. Section IV evaluates the performance of our method from system throughput and detection probability. Concluding the paper, Section V offers final observations.

## II. System Model

Given that the NOMA and sensing challenges in large-scale IoT primarily pertain to the uplink scenario, this paper centers on the uplink system. As illustrated in Fig. 1, in our system model, the primary power-domain NOMA system comprises $N$ primary users, while the neighboring terrestrial IoT terminals constitute the secondary system. We focus on studying the performance of the secondary user in detecting the transmission states of multiple primary users to facilitate the rational use of spectral holes. In short, the secondary user (SU) need through spectrum sensing to determine if the target primary user (PU) is currently occupying the spectrum resources.

Referring to the leading studies concerning power-domain NOMA, in this model, it is assumed that user $i$ transmits with signal $x_i, i = 1, \ldots, N$ and transmit power $p_i, p_i = \beta_i p, \beta_i > 0, \sum_{i=1}^{N} \beta_i = 1, \sum_{i=1}^{N} p_i \leq 1$, [45], [46]. The $p$ denotes the maximum system total power.

We apply the feature-based spectrum sensing method in this paper, which compares the accumulation of features with a pre-determined threshold. To obtain the signal's features, the Cyclic Delay Diversity (CDD) technology is used. Compared to the mainstreamed feature detection scheme based on reference signal and subcarrier mapping, the use of CDD, on one hand, reduces the dependence on the prior information of the PU, and on the other hand, reduces the additional spectral resource overhead while enabling additional diversity gain with the help of multiple antenna configurations [47], [48].

Two transmit antennas are utilized for the PU and a single receive antenna is used for the SU. The transmitter operates by generating signals directly from one antenna, adding a cyclic prefix after coding and modulation, and then transmitting. The signal from the second antenna undergoes a cyclic shift based on an artificial cyclic delay before the addition of a cyclic prefix. The signals transmitted from both antennas can be characterized as

$$t_1(n) = \frac{1}{\sqrt{2M}} \sum_{r=-\infty}^{+\infty} v(n - rT) \sum_{x=0}^{M-1} a_{r,x} W_M^{x((r+1)T-n)} \quad (1)$$

and

$$t_2(n) = \frac{1}{\sqrt{2M}} \sum_{r=-\infty}^{+\infty} v(n - rT) \sum_{x=0}^{M-1} a_{r,x} W_M^{x((r+1)T-n)} W_M^{x\Delta}, \quad (2)$$

respectively. Where $\Delta$ represents the cyclic delay, $M$ denotes the number of carriers, $T$ is the total length of carriers and cyclic prefix, $W_M = e^{\frac{-j2\pi}{M}}$, $a_{r,x}$ represents the data on the $r$-th symbol and $x$-th carrier of an Orthogonal Frequency-Division Multiplexing (OFDM) signal, and the function $v(n)$ can be written as

$$v(n) = \begin{cases} 1 & n = 0, 1, \ldots, T-1 \\ 0 & \text{otherwise.} \end{cases} \quad (3)$$

At the receiver, the process of spectrum sensing can be seen as a binary hypothesis testing problem. With a single antenna, the received signal can be expressed as

$$r(n) = \begin{cases} w(n), & H_0 \\ \mathbf{ht}(n) + w(n), & H_1 \end{cases} \quad (4)$$

where $H_0$ denotes PU is not transmitting while $H_1$ represents the existence of PU's signal, and $\mathbf{h} = [h_1, h_2]$ is the discrete-time channel impulse response, $\mathbf{t}(n) = [t_1(n), t_2(n)]^T$ is transmitted OFDM signals with $w(n)$ denoting the Additive White Gaussian Noise (AWGN). Then, the decision can be designed as

$$\begin{cases} \tilde{H}_0 : |F| < \xi \\ \tilde{H}_1 : |F| \geq \xi, \end{cases} \quad (5)$$

where $\xi$ represents the given false-alarm threshold while $\tilde{H}_0$ and $\tilde{H}_1$ denote the absence and existence of PU, respectively. $|F|$ represents the feature value of the received signal, which can be calculated as

$$|F| = \left| \frac{1}{T} \sum_{n=0}^{T-1} r(n) r^*(n + \Delta) \right|. \quad (6)$$

Thus, we have the detection probability ($P_d$) and the false-alarm probability ($P_f$) as

$$\begin{aligned} P_d &= \Pr\left(\tilde{H}_1 \mid H_1\right) \\ &= \Pr(|F| \geq \xi) \\ &= \Pr\left(\left| \frac{1}{T} \sum_{n=0}^{T-1} r(n) r^*(n + \Delta) \right| \geq \xi\right) \end{aligned} \quad (7)$$

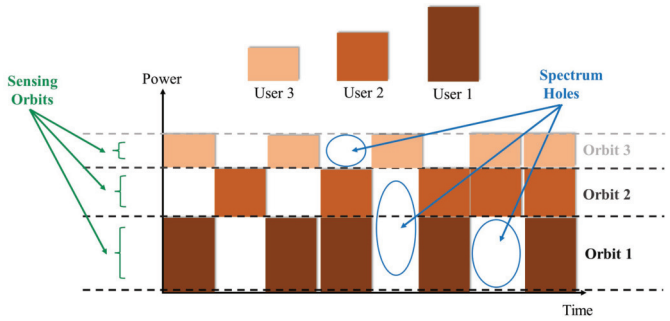


Fig. 2. Conceptual diagram of spectrum resources and orbital distribution for N-users (a case with three users).

and

$$\begin{aligned} P_f &= \Pr\left(\tilde{H}_1 \mid H_0\right) \\ &= \Pr(|F| \geq \xi) \\ &= \Pr\left(\left|\frac{1}{T}\sum_{n=0}^{T-1} w(n)w^*(n+\Delta)\right| \geq \xi\right). \end{aligned} \tag{8}$$

These two metrics are interdependent, a low $P_f$ indicates that the SU is sharing spectrum resources extensively, whereas a high $P_d$ reduces interference to the PU's signals. However, increasing the $P_d$ or decreasing the $P_f$ tends to affect another metric simultaneously. Therefore, our objective is to achieve a high $P_d$ while keeping the $P_f$ at a minimum level.

## III. Proposed Method

In this section, we first design the basic workflow of the spectrum sensing, then we explore the $P_f$ fluctuation problem under transmitting uncertainty with proposed-I method. After that, we design the proposed-II method to conquer this challenge and derive the corresponding threshold theoretically.

### A. The Basic Workflow Design and Derivation of False-Alarm Probability

Fig. 2 shows a conceptual diagram of the spectral holes and orbit resources of a NOMA system with three users. We can see that in power-domain NOMA, different users are distinguished from each other by power and they can share the same time-frequency resource block. The traditional spectral holes can be considered as the resource block in the target frequency band that is not occupied by users, while in NOMA system, in addition to the existence of such traditional spectral holes, there is actually a non-fully occupied spectral holes. Specifically, when the number of shared users under a certain target time-frequency resource in the NOMA system does not reach the upper limit, meanwhile, the SU can communicate with the base station constituting NOMA through the appropriate power, which achieves the purpose of making full use of the spectrum resources without affecting the transmission of the PUs. In this way, different users have different power and correspond to different cyclic delay features, thus we can visualize the spectrum resources in the system in the form of orbitals, which can be used to detect the state information of the non-full-occupancy spectral holes.

Considering $N$ users in the primary system, we assume that $n$ denotes the sampling point, the transmitted signal can be written as

$$t_i^1(n) = \sqrt{p_i}x_i(n), \tag{9}$$

and

$$t_i^2(n) = \sqrt{p_i}x_i(n+\Delta_i), \tag{10}$$

respectively. $\Delta_i$ denotes the cyclic delay of User $i$.

The SU receives signals through Rayleigh channels $\mathbf{h}$, with each user in the primary system transmitting signals independently and randomly. To simplify calculations, we assume a decreasing power trend from User 1 to User $N$, where User 1 has the strongest power and User $N$ has the weakest power. To begin with the worst-case scenario, we focus on sensing the state of User $m$ while all other PUs are transmitting signals. The interference signal in the $H_1$ situation can be expressed as

$$r(n) = \sum_{i=1}^{N} \Phi_i \mathbf{h}_i \mathbf{t}_i(n) + w(n), \tag{11}$$

where $\Phi_i$ stands for the transmit state of User $i$, the probability can be denoted as

$$\begin{cases} P\left(\Phi_i = 1\right) = \phi_i, \\ P\left(\Phi_i = 0\right) = 1 - \phi_i, \end{cases} \tag{12}$$

where $\phi$ $(0 < \phi < 1)$ is probability of User $i$ transmitting.

Then the $P_f$ can be obtained by

$$\begin{aligned} P_f &= \Pr\left(|F\left(\Delta_m\right)| \geq \xi\right) \\ &= \Pr\left(\left|\frac{1}{T}\sum_{n=0}^{T-1} r_m(n) r_m^*\left(n+\Delta_m\right)\right| \geq \xi\right). \end{aligned} \tag{13}$$

We suppose that all users exist except User $m$. To calculate the relationship between $P_f$ and $\xi$, let $C_m = r_m(n)r_m^*\left(n+\Delta_m\right)$, which can be further expressed as Eqn.(24), shown at the bottom of the next page. The distributions of the 4 parts can be calculated as follows:

Choosing Quadrature Phase Shift Keying (QPSK) modulation and Rayleigh channel, we have

$$\begin{cases} t_i(n) = \dfrac{\sqrt{p_i}}{2} t_i = \dfrac{\sqrt{p}}{2}\left(n_j + \mathrm{i}m_j\right), \\ w(n) = \dfrac{N_0}{\sqrt{2}} w = \dfrac{N_0}{\sqrt{2}}\left(c_j + \mathrm{i}d_j\right), \\ h(n) = \dfrac{1}{\sqrt{2}} h = \dfrac{1}{\sqrt{2}}\left(a_j + \mathrm{i}b_j\right), \end{cases} \tag{14}$$

where $a_j, b_j$, $c_j$ and $d_j$ are independent identically distributed (i.i.d.) variables that obey the standard normal distribution. $m_j, n_j = \pm 1$.

1) Let $C_I = w(n)w(n+\Delta_m)^*$ and can be written as

$$C_I = \frac{N_0^2}{2} w_1 w_2^* = \frac{N_0^2}{2}\left[\left(c_1c_2 + d_1d_2\right) + \mathrm{i}\left(c_2d_1 - c_1d_2\right)\right] \tag{15}$$

We can obtain that the probability mean and probability variance of the real and imaginary parts, which can be written as

$$\begin{cases} \mu_{C_I I} = \mu_{C_I R} = 0, \\ \sigma_{C_I I}^2 = \sigma_{C_I R}^2 = \dfrac{N_0^4}{2}. \end{cases} \tag{16}$$

2) The $C_{II}$ components is as below

$$C_{II}=\sum_{i\neq m}^{N}\mathbf{h}_i\mathbf{t}_i(n)w^*(n+\Delta_m)+\sum_{i\neq m}^{N}\mathbf{h}_i^*\mathbf{t}_i^*(n+\Delta_m)\,w(n). \tag{17}$$

Let $\tilde{C_{II}}=\mathbf{h}_i^*\mathbf{t}_i^*(n+\Delta_m)w(n)+\mathbf{h}_i\mathbf{t}_i(n+\Delta_m)w(n+\Delta_m)^*$, and we have

$$\begin{aligned}\tilde{C_{II}}&=\frac{\sqrt{p_i}N_0}{4}\left(\left(h_1t_1+h_2t_2\right)w_1+\left(h_3t_3+h_4t_4\right)w_2\right)\\&=\frac{\sqrt{P_i}N_0}{4}\left(\left(a_1+\mathrm{i}b_1\right)\left(m_1+\mathrm{i}n_1\right)\right.\\&\quad\left.+\left(a_2+\mathrm{i}b_2\right)\left(m_2+\mathrm{i}n_2\right)\right)\left(c_1+\mathrm{i}d_1\right)\\&=a_1m_1c_1-b_1n_1c_1+a_2m_2c_1-b_2n_2c_1\\&\quad-a_1n_1d_1-b_1m_1d_1-a_2n_2d_1-b_2m_2d_1\\&\quad+\mathrm{i}\left(a_1n_1c_1+b_1m_1c_1+a_2n_2c_1+b_2m_2c_1\right.\\&\quad\left.+a_1m_1d_1-h_1n_1d_1+a_2m_2d_1-b_2n_2d_1\right).\end{aligned} \tag{18}$$

Similarly, the mean and variance of $\tilde{C_{II}}$ can be obtained as

$$\begin{cases}\mu_{\tilde{C_{II}}I}=\mu_{\tilde{C_{II}}R}=0,\\ \sigma^2_{\tilde{C_{II}}I}=\sigma^2_{\tilde{C_{II}}R}=p_iN_0^2.\end{cases} \tag{19}$$

Since the terms in $C_{II}$ are independent and uncorrelated with each other, we have

$$\begin{cases}\mu_{C_{II}I}=\mu_{C_{II}R}=0,\\ \sigma^2_{C_{II}I}=\sigma^2_{C_{II}R}=\sum_{i\neq m}^{N}p_iN_0^2.\end{cases} \tag{20}$$

3) Following is the multiplication of signals from the same users

$$C_{III}=\sum_{i\neq m}^{N}\mathbf{h}_i\mathbf{t}_i(n)\mathbf{h}_i^*\mathbf{t}_i^*\left(n+\Delta_m\right). \tag{21}$$

Similarly, we have

$$\begin{aligned}\tilde{C_{III}}&=\mathbf{h}_i\mathbf{t}_i(n)\mathbf{h}_i^*\mathbf{t}_i^*\left(n+d_k\right)\\&=\frac{p_i}{8}\left(\left|h_1\right|^2t_1t_2^*+\left|h_2\right|^2t_3t_4^*\right.\\&\quad\left.+h_1h_2^*t_1t_4^*+h_1^*h_2t_2t_3^*\right).\end{aligned} \tag{22}$$

Let $\tilde{C_{III1}}=\left|h_1\right|^2t_1t_2^*,\tilde{C_{III2}}=\left|h_2\right|^2t_3t_4^*,\tilde{C_{III3}}=h_1h_2^*t_1t_4^*,\tilde{C_{III4}}=h_1^*h_2t_2t_3^*$, notice that $C_{III1},C_{III2}$ have the same probability distribution, as well as $\tilde{C_{III3}},\tilde{C_{III4}}$. Thus, for $\tilde{C_{III1}}$, we know that $P(t_1t_2^*=\pm2,\pm2\mathrm{i})=\frac{1}{4}$ and $\left|h_1\right|^2=a_1^2+a_2^2\sim\mathcal{X}^2(2)$, we get $\mu_{\tilde{C_{III1}}}=0,\sigma^2_{\tilde{C_{III1}}}=16$.
For $\tilde{C_{III4}}$, similarly, we get $\mu_{\tilde{C_{III3}}}=0,\sigma^2_{\tilde{C_{III3}}}=8$. Therefore, we have the $C_{III}$ following

$$\begin{cases}\mu_{C_{III}I}=\mu_{C_{III}R}&=0,\\ \sigma^2_{C_{III}I}=\sigma^2_{C_{III}R}&=\sum_{i\neq m}^{N}\frac{3}{4}p_i^2.\end{cases} \tag{23}$$

4) Finally, the multiplication of signals from different users is

$$C_{IV}=\sum_{i\neq m}^{N}\sum_{\substack{j\neq m\\ j\neq i}}^{N}\mathbf{h}_i\mathbf{t}_i(n)\cdot\mathbf{h}_j^*\mathbf{t}_j^*\left(n+\Delta_m\right). \tag{25}$$

Suppose that

$$\begin{aligned}\tilde{C_{IV}}&=\mathbf{h}_i\mathbf{t}_i(n)\cdot\mathbf{h}_j^*\mathbf{t}_j^*\left(n+\Delta_m\right)\\&=\frac{\sqrt{p_ip_j}}{8}\left(h_1t_1+h_2t_2\right)\left(h_3t_3+h_4t_4\right)^*.\end{aligned} \tag{26}$$

Similarly, we have $\mu_{\tilde{C_{IV}}}=0,\sigma^2_{\tilde{C_{IV}}}=\frac{p_ip_j}{2}$. Thus, $C_{IV}$ obey

$$\begin{cases}\mu_{C_{IV}}=0\\ \sigma^2_{C_{IV}}=\sum_{i\neq m}^{N}\sum_{\substack{j\neq m\\ j\neq i}}^{N}\frac{p_ip_j}{2}.\end{cases} \tag{27}$$

In summary, consider the four components of $C_m$, the distribution of the real and imaginary parts can be written as

$$\begin{cases}\mu_{C_m}=0\\ \sigma^2_{C_m}=\frac{1}{2}N_0^4+\sum_{i\neq m}^{N}\left(p_iN_0^2+\frac{3}{4}p_i^2+\sum_{\substack{j\neq m\\ j\neq i}}^{N}\frac{1}{2}p_ip_j\right).\end{cases} \tag{28}$$

According to the Law of Large Numbers, the distribution of $F(\Delta_m)$ can be expressed as

$$\dot{I}_{F(\Delta_m)},\dot{Q}_{F(\Delta_m)}\sim N\left(0,\frac{\sigma^2_{C_m}}{T}\right). \tag{29}$$

Thus, let $u=\left|F\left(\Delta_m\right)\right|$. It follows a Rayleigh distribution, the according probability distribution can be defined as

$$f(u)=\frac{uT}{\sigma^2_{C_m}}e^{\frac{-u^2T}{2\sigma^2_{C_m}}}(u\geq0). \tag{30}$$

$$\begin{aligned}C_m&=\left[\sum_{i\neq m}^{N}\mathbf{h}_i\mathbf{t}_i(n)+w(n)\right]\left[\sum_{i\neq m}^{N}\mathbf{h}_i\mathbf{t}_i\left(n+\Delta_m\right)+w\left(n+\Delta_m\right)\right]^*\\&=\underbrace{\sum_{i\neq m}^{N}\mathbf{h}_i\mathbf{t}_i(n)\sum_{i\neq m}^{N}\mathbf{h}_i^*\mathbf{t}_i^*\left(n+\Delta_m\right)}_{C_{\mathrm{III}}\text{ and }C_{\mathrm{IV}}\text{ components}}+\underbrace{\sum_{i\neq m}^{N}\mathbf{h}_i\mathbf{t}_i(n)w^*\left(n+\Delta_m\right)+\sum_{i\neq m}^{N}\mathbf{h}_i^*\mathbf{t}_i^*\left(n+\Delta_m\right)w(n)}_{C_{\mathrm{II}}\text{ components}}+\underbrace{w(n)w^*\left(n+\Delta_m\right)}_{C_{\mathrm{I}}}.\end{aligned} \tag{24}$$

Then we have the $P_f$ calculated by

$$\begin{aligned} P_f &= \Pr\left(\left|\frac{1}{T}\sum_{n=0}^{T-1} r_m(n) r_m^*(n+\Delta_m)\right| \geq \xi\right) \\ &= \int_{\xi}^{+\infty} \frac{uT}{\sigma_{C_m}^2} e^{\frac{-u^2 T}{2\sigma_{C_m}^2}} du \\ &= e^{\frac{-\xi^2 T}{2\sigma_{C_m}^2}}. \end{aligned} \tag{31}$$

The threshold can be expressed as

$$\xi = \sqrt{-2\frac{\ln(P_f)}{T}\sigma_{C_m}^2}. \tag{32}$$

### *B. The Phenomenon of False-Alarm Probability Fluctuation Under Transmitting Uncertainty*

For SU, the transmitting probability of the $N$ users in the primary system is uncertainty. We preliminarily proposed a detection method which assumes that there is user-noise superimposed interference or noise-only interference.

Specifically, if there is only noise exist, the $P_f$ can be calculated by Eqn.(8), and following the similar process, the threshold can be written as

$$\xi = \sqrt{-\frac{\ln P_f}{T}(N_0^4)}. \tag{33}$$

While if there is only one PU exist, the $r(n)$ and $P_f$ can be expressed as

$$\begin{cases} r(n) = \mathbf{h}_m \mathbf{t}_m(n) + w(n), \\ P_f = \Pr\left(\left|\frac{1}{T}\sum_{n=0}^{T-1} r(n) r^*(n+\Delta_m)\right| \geq \xi\right). \end{cases} \tag{34}$$

Then we have the threshold based on Eqn.(28)

$$\xi = \sqrt{-\frac{\ln P_f}{T}\left(N_0^4 + 2N_0^2 p_j + \frac{3}{2}p_j^2\right)} (j \neq m, j \in 1 \to N), \tag{35}$$

The specific process is showed in Algorithm 1, of which the complexity is O($N \times T$), linear with the number of users and sensing window. For the sake of distinction, we regard this method as proposed-I. However, if the PUs' number $N \geq 3$, with the increasing of uncertainty, proposed-I can not stabilize the fluctuation of $P_f$, which can be seen at Fig. 3 and Fig. 4. With the Signal-to-Noise Ratio (SNR) increasing, the $P_f$ fluctuation is getting worse. Meanwhile, proposed-I lake of adjustment capacity and different thresholds settings result in different $P_f$ fluctuation degree.

### *C. Presentation of the Orbital Estimation and Design of Proposed-II*

To mitigate the effects of uncertainty, a two-step strategy involving the introduction of the concept of orbit is proposed. This strategy entails initially estimating the orbits to ascertain whether a user is transmitting information on each orbit, followed by conducting precise detection based on the estimation results, referred to as proposed-II. Fig. 2 illustrates the allocation of spectrum resources and orbits in a three-primary user NOMA system, with each orbit representing a distinct combination of power and cyclic delay resources. As depicted in Fig. 5, following the acquisition of feature values, the outcomes of orbit estimation are categorized into four

**Algorithm 1** Multi-User Detection Method With Transmitting Uncertainty Based on Single Orbit-Proposed I

**Input**: the number of primary users: $N$;
the transmitting power of users: $p_m$;
the cyclic delays of each user: $\Delta_m$;
sensing window length: $T$;
the environment $SNR$.

**Initialize the parameters randomly**;
PUs send messages at random, while SU receives the signal $r$ from PUs in each time slot.
**if** *the SU wants to share the spectrum* **then**
  Choose sensing target User $m$ ($m \in 1 \to N$);
  **for** *each time slot* **do**
    Calculating decision threshold with cyclic shift
    **if** $m \neq N$ **then**
      $\xi_m = \sqrt{-\frac{\ln P_f}{T}\left(N_0^4 + 2N_0^2 p_j + \frac{3}{2}p_j^2\right)}$
      $(j = m+1)$
    **else**
      $\xi_m = \sqrt{-\frac{\ln P_f}{T}\left(N_0^4 + 2N_0^2 p_1 + \frac{3}{2}p_1^2\right)}$
    If we consider noise interference only:
    $\xi_m = \sqrt{-\frac{\ln P_f}{T}(N_0^4)}$;
    Calculate the feature value of received signal $r$:
    $F_m = \frac{1}{T}\sum_{n=0}^{T-1} r(n) r^*(n+\Delta_m)$;
    **if** $|F_m| < \xi_m$ **then**
      User $m$ is not occupying the channel resource;
      The SU transmits the signal in NOMA mode with power no more than $p_m$
    **else**
      User $m$ is occupying the channel resource;
      The SU need to wait for next sensing operation

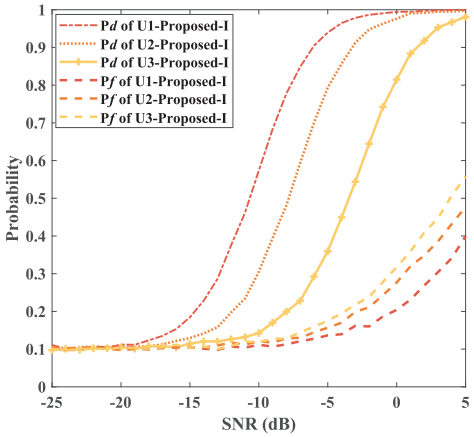


Fig. 3. $P_d$ and $P_f$ comparison in three-user PUs NOMA system under uncertainty PU transmitting probability with proposed-I method (suppose only noise interference).

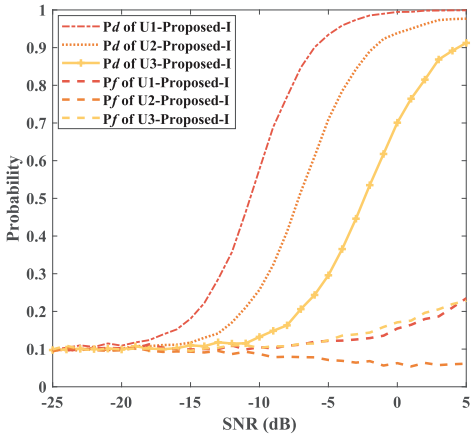


Fig. 4. $P_d$ and $P_f$ comparison in three-user PUs NOMA system under uncertainty PU transmitting probability with proposed-I method (suppose single user and noise interference).

distinct types. In the event that all orbits are unoccupied, the SU is able to utilize the frequency band for transmission without interference. Conversely, if all three orbits are occupied, transmission must be ceased. In cases where partial orbits are occupied, a more precise false alarm threshold must be established based on the orbit estimation findings to facilitate an accurate decision-making process, ultimately leading to the selection of the orbit with the highest power level for transmission.

$$r_1(n)=\begin{cases}\Phi_2\mathbf{h}_2\mathbf{t}_2(n)+\Phi_3\mathbf{h}_3\mathbf{t}_3(n)+w(n), & H_0\\ \mathbf{h}_1\mathbf{t}_1(n)+\Phi_2\mathbf{h}_2\mathbf{t}_2(n)+\Phi_3\mathbf{h}_3\mathbf{t}_3(n)+w(n), & H_1\end{cases} \tag{36}$$

Step 1: Orbit estimation.

For the situation $H_0$, we need to determine the value of $\Phi_i(i=2,3)$. Notice that in the three-PU system, each orbit has three occupying states, for example, estimate the orbit 1, only User 2 or User 3 is existing and both User 2 and 3 are existing, similar to the other orbits.

Similarly, based on the derivation of III-A, we can get the feature value $F(\Delta_1)$ by

$$F(\Delta_1)=\left|\frac{1}{T}\sum_{n=0}^{T-1} r_1(n)r_1^*(n+\Delta_1)\right|. \tag{37}$$

Then, according to Eqn.(28), the probability distribution of $F(\Delta_1)$ can be calculated as

$$\begin{cases}\mu_{C_1}=0\\ \sigma^2_{C_1}=\dfrac{1}{2}N_0^4+\displaystyle\sum_{i\neq 1}^{3}\left(p_iN_0^2+\frac{3}{4}p_i^2+\sum_{\substack{j\neq 1\\ j\neq i}}^{3}\frac{1}{2}p_ip_j\right)\end{cases}. \tag{38}$$

For the threshold, we consider all occupying situation and apply arithmetic mean to calculate the estimation threshold, which can be defined as

$$\xi_e=\frac{1}{3}\left(\sum_{\substack{j\neq k\\ j=1}}^{3}\sqrt{-\frac{\ln P_f}{T}\left(N_0^4+2N_0^2p_j+\frac{3}{2}p_j^2\right)}\right.$$
$$\left.+\sqrt{-\frac{\ln P_f}{T}\left(N_0^4+\sum_{\substack{n\neq k\\ n=1}}^{3}\left(2N_0^2p_n+\frac{3}{2}p_n^2+\sum_{\substack{t\neq k\\ t=1\\ t\neq n}}^{3}p_np_t\right)\right)}\right), \tag{39}$$

where $k$ denotes the orbit which is estimated ($k=1$ to estimate orbit 1). While if for $N$-PUs system, let $\beta=N-i+1$, $\xi_e$ can be changed as

$$\xi_e=\frac{1}{2N-3}\left(\sum_{\substack{j\neq k\\ j=1}}^{N}\sqrt{-\frac{\ln P_f}{T}\left(N_0^4+2N_0^2p_j+\frac{3}{2}p_j^2\right)}\right.$$
$$\left.+\sum_{i=2}^{N-1}\sqrt{-\frac{\ln P_f}{T}\left(N_0^4+\sum_{\substack{n\neq k\\ n=\beta}}^{N}\left(2N_0^2p_n+\frac{3}{2}p_n^2+\sum_{\substack{t\neq k\\ t=\beta\\ t\neq n}}^{N}p_np_t\right)\right)}\right). \tag{40}$$

Finally, if $F(\Delta_1>\xi_e)$, we set the $\Phi_1=1$ to denote orbit 1 is occupying.

Step 2: Precise decision.

After determining the state of orbits, we have access to identified signal interference in Eqn.(36). Then the new threshold with $\Phi_i$ can be written as

$$\xi_1=\sqrt{-2\frac{\ln P_f}{T}\left(0.5\ N_0^4+\sum_{i\neq 1}^{3}\Gamma(i)\right)}, \tag{41}$$

where $\Gamma(i)$ can be defined as

$$\Gamma(i)=\left(\Phi_ip_iN_0^2+\Phi_i\frac{3}{4}p_i^2+\sum_{\substack{j\neq 1\\ j\neq i}}^{3}\frac{1}{2}p_ip_j\Phi_i\Phi_j\right). \tag{42}$$

The specific process can be seen in Algorithm 2, of which the complexity is $\mathrm{O}(N^2+N\times T)$, quadratic in terms of users due to orbit estimation and decision process.

To provide a more comprehensive representation of the proposed method's performance, we incorporate the system throughput, encompassing both the PU and SU, which can further illustrate the superiority of the proposed method. The average system throughput with $N$ users can be written as

$$R=\left[\prod_{i=1}^{m-1}\Pr\left(H_1^{(i)}\right)\right]\Pr\left(H_0^{(m)}\right)(1-P_f)\,R_{SU}^{(m)}$$
$$+\sum_{\substack{i\neq m\\ i=1}}^{N}\Pr\left(H_1^{(i)}\right)R_{PU}^{(i)}, \tag{43}$$

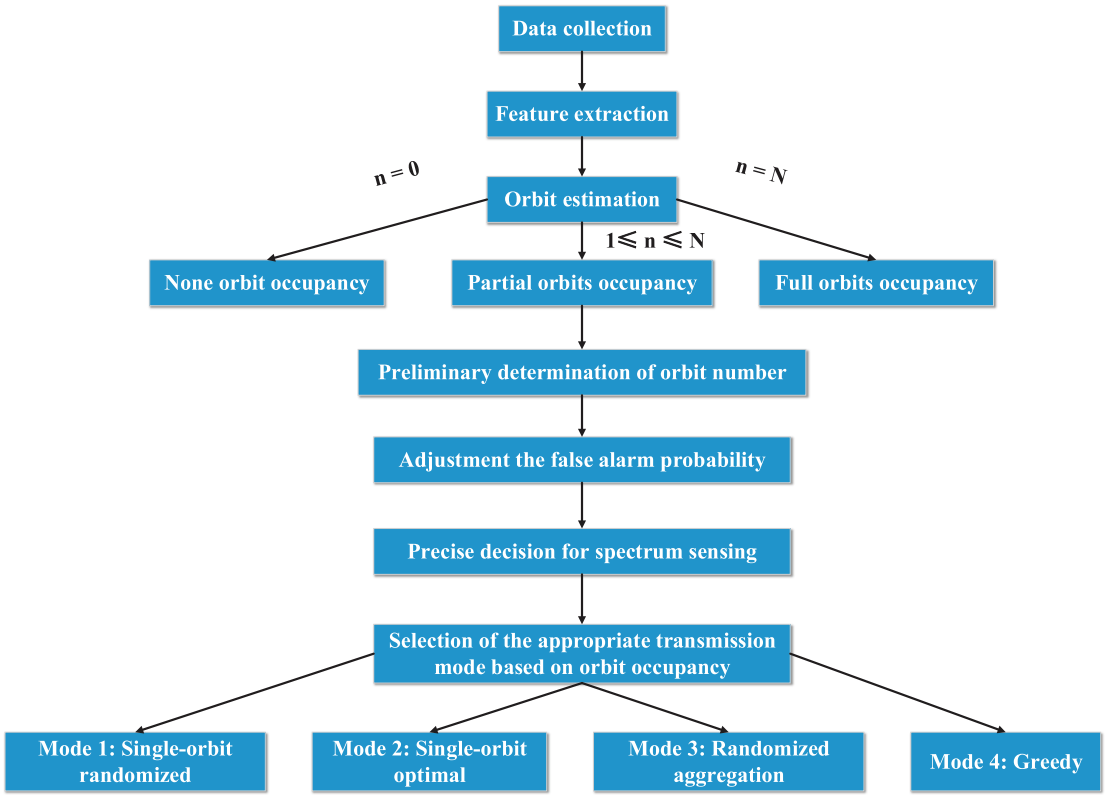


Fig. 5. Flow chart of multi-user detection method with orbit estimation (proposed-II): a case with three NOMA users.

where $\Pr\left(H_1^{(i)}\right)$ denotes the probability of User $i$ transmitting while $\Pr\left(H_0^{(m)}\right)$ represents that user $m$ does not send messages. $R_{SU}^{(m)}$ and $R_{PU}^{(i)}$ can be defined as

$$R_{SU}^{(m)} = \log\left(1 + \frac{p_m \left|h_m\right|^2}{\sum_{j=m+1}^{N} \Phi_j p_j \left|h_j\right|^2 + \sigma_n^2}\right), \tag{44}$$

and

$$R_{PU}^{(i)} = \log\left(1 + \frac{p_i \left|h_i\right|^2}{\sum_{j=i+1}^{N} \Phi_j p_j \left|h_j\right|^2 + \sigma_n^2}\right). \tag{45}$$

## IV. Simulation Results

In this section, the performance superiority of the proposed method is illustrated through numerical results. A benchmark of $P_f$ is established at 0.1 using the Monte Carlo method to calculate the detection probability and throughput. Without loss of generality, the simulations in this paper are based on 3-user scenarios that are widely adopted [49], [50], which can be further extended to more user scenarios based on the derivations in the previous sections and practical requirements. It is worth noting that the transmission probability of each user in the primary system is set to be random and uncorrelated in the present context. The SU must conduct spectrum sensing and access unauthorized frequency bands without prior knowledge of the transmission probabilities of the PU.

The proposed system utilizes orbit estimation to determine the overall utilization of orbital resources, facilitating the selection of resources with the most efficient power for transmission in power-domain NOMA systems. The power allocation ratio of PUs in our work is $5:3:1$. In addition to the given centralized strategy that imposes a total power constraint across all users, practical applications also involve decentralized strategies, where the power of each user is optimized individually [51], [52]. Thus in this section, we conduct comprehensive simulations to evaluate both two strategies, specifically considering uplink scenarios with and without user power normalization to provide a more holistic understanding of power optimization within the framework of the proposed method. In this study, we utilize the most recent NOMA techniques as a benchmark [34], [41], [42], referred to as the "NOMA-benchmark" method, which stands for the NOMA technologies without the ability to sense. Specific parameters can be found in Table I.

TABLE I
Simulation Parameters

| Parameters | Values |
|---|---|
| Signal size | 4096 |
| Channel coding | $LDPC$ |
| Coding rate | $449/1024$ |
| Antenna configuration | $2 \times 1$ |
| Channel model | Rayleigh channel |
| Number of PUs | 3 |
| Power ratio | $p_1 : p_2 : p_3 = 5:3:1$ |
| Modulation | QPSK |
| False alarm probability | 0.1 |

Fig. 6 to Fig. 10 consider the user-noise superimposed interference situation in proposed-I. Fig. 6 depicts the proba-

**Algorithm 2** Multi-User Detection Method With Transmitting Uncertainty Based Orbit Estimation-Proposed-II

**Input**: the number of users: $N$;
the transmitting power of users: $p_m$;
the cyclic delays of each user: $\Delta_m$;
sensing window length: $T$;
the environment $SNR$.

**Initialize the parameters randomly**;
PUs send messages at random, while SU receives the signal $r$ from PUs in each time slot.
**Stage1: Orbit estimation:**
**if** *the SU wants to share the spectrum* **then**
  **for** *orbit* $k = 1$ *to* $N$ **do**
    Setting decision threshold

$$\xi_{ek} = \frac{1}{2N-3}\left(\sum_{\substack{j\neq k\\ j=1}}^{N}\sqrt{-\frac{\ln P_f}{T}\left(N_0^4 + 2N_0^2 p_j + \frac{3}{2}p_j^2\right)}\right.$$
$$\left. + \sum_{i=2}^{N-1}\sqrt{-\frac{\ln P_f}{T}\left(N_0^4 + \sum_{\substack{n\neq k\\ n=\beta}}^{N}\left(2N_0^2 p_n + \frac{3}{2}p_n^2 + \sum_{\substack{t\neq k\\ t=\beta\\ t\neq n}}^{N} p_n p_t\right)\right)}\right).$$

    Calculate the feature value of received signal $r$:
    $F(\Delta_k) = \left|\frac{1}{T}\sum_{n=0}^{T-1} r_k(n) r_k^*(n+\Delta_k)\right|$;
    **if** $F(\Delta_k) < \xi_{ek}$ **then**
      Orbit $i$ is not occupied;
      The corresponding flag $\Phi_k = 0$.
    **else**
      The corresponding flag $\Phi_k = 1$.
**Stage2: Precise decision:**
**for** *User* $m = 1$ *to* $N$ **do**
  $\Gamma(j) = \left(\Phi_j p_j N_0^2 + \Phi_j \frac{3}{4} p_j^2 + \sum_{\substack{i\neq j\\ i\neq m}}^{N} \frac{1}{2} p_i p_j \Phi_i \Phi_j\right)$;
  $\xi_m = \sqrt{-2\frac{\ln P_f}{T}\left(0.5\ N_0^4 + \sum_{j\neq m}^{N}\Gamma(j)\right)}$;
  **if** $F(\Delta_m) < \xi_m$ **then**
    User $m$ is not transmitting;
    The SU can occupy this spectrum resource to send signal in NOMA mod with power no more than $p_m$
  **else**
    User $m$ is transmitting;
    Break;

bility of detection for the SU in a three-primary user uplink NOMA system, with a power allocation ratio of 5 : 3 : 1. The detection performance of the SU varies among User 1, User 2, and User 3 due to the interference from each PU. User 1, having the highest proportion of transmission power, experiences less impact from signal interference from other PUs, resulting in optimal detection performance. The detection probability reaches 80% at an overall SNR of approximately -8 dB. However, the proposed method demonstrates subpar detection performance as a result of the limited transmit power allocation for User 3, with the detection probability reaching 80% at an SNR of approximately 3 dB.

Furthermore, when the other two high-power primary users are transmitting, the interference experienced by User 3 is exacerbated, potentially causing the feature peaks to be obscured. The proposed-I method also demonstrates inadequate performance in terms of the detection probability of User 3, achieving only approximately 80% at an SNR of 2 dB. Regarding $P_f$, it is apparent that the proposed-I method starts to fluctuate once the SNR surpasses -10 dB, with the deviation from 0.1 progressively growing as the SNR increases. The proposed-I method fails to account for the variability in the transmission signals of the PU, resulting in fluctuating $P_f$ values and a high likelihood of false positives. In contrast, the proposed-II method mitigates the influence of unknown factors through orbit estimation, enabling more precise decision-making and improved fault tolerance, ultimately maintaining $P_f$ at approximately 0.1. These measures effectively reduce the impact of PU's transmission randomness on detection performance.

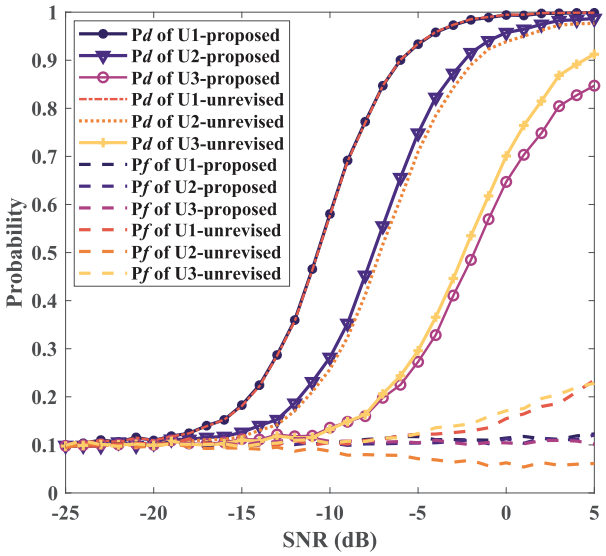


Fig. 6. $P_d$ and $P_f$ comparison in three-user PUs NOMA system with the preliminary and proposed method under uncertainty PU transmitting probability with user interference (no $P_f$ revision).

Fig. 7 displays the performance comparison between the proposed-II method and a modified version of the proposed-I method. In the proposed-I method, the threshold was manually adjusted to maintain a $P_f$ of approximately 0.1. For the normalization case, the proposed-II method exhibited a detection performance improvement of up to 9.5% for User 2 compared to the proposed-I method within the SNR range of -10 dB to -5 dB. Following the adjustment, the $P_d$ for User 3 was effectively constrained, reaching 80% at approximately 5 dB. Following the adjustment process, the falsely elevated $P_d$ value of User 3 was mitigated and stabilized at 80% at approximately 5 dB. Furthermore, User 3 experienced a noticeable enhancement of approximately 4% within the range of 0 dB to 5 dB. These results indicate that the proposed-II scheme exhibits superior detection performance compared to the adjusted proposed-I scheme.

Meanwhile, Fig. 7a (the non-normalized case) reveals a higher $P_d$ compared to Fig. 7b (the normalized case) at the same SNR. For instance, at an SNR of -10 dB, $P_d$ for the

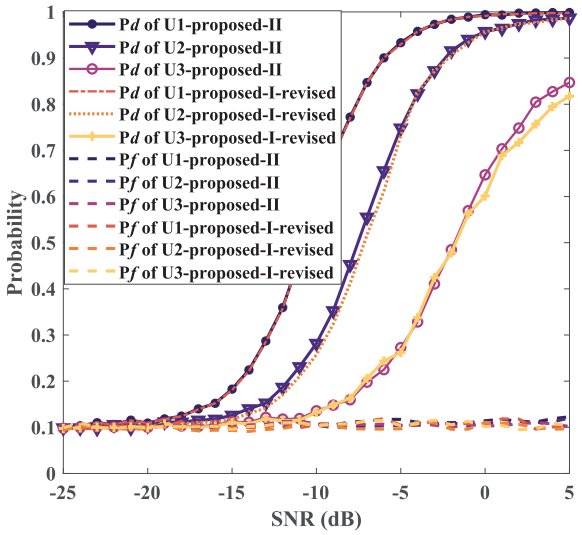


(a) Results with user energy normalization.

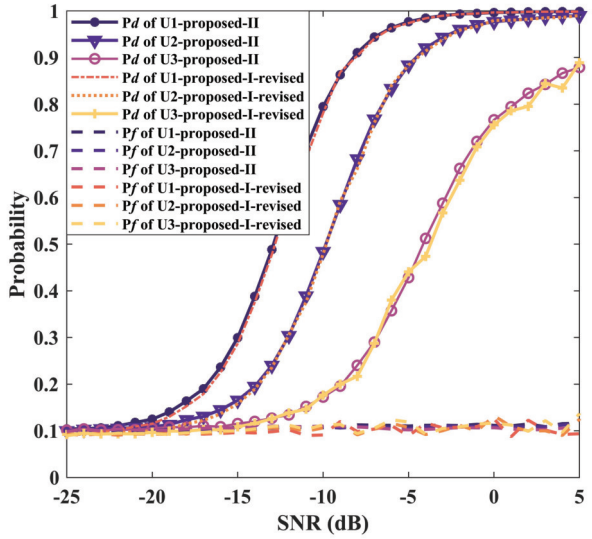


(b) Results without user energy normalization.

Fig. 7. $P_d$ and $P_f$ comparison in three-user PUs NOMA system with the preliminary and proposed method under uncertainty PU transmitting probability with user interference.

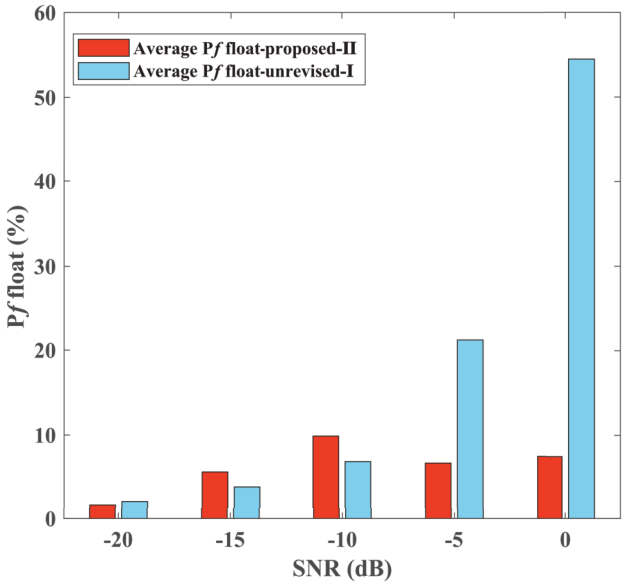


(a) Results with user energy normalization.

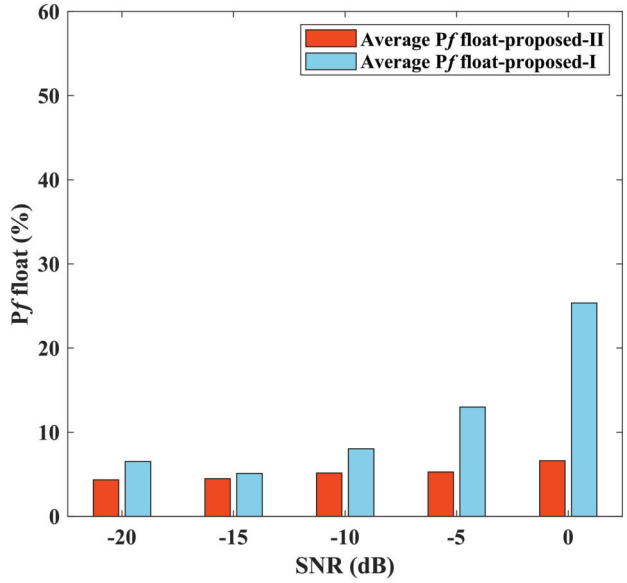


(b) Results without user energy normalization.

Fig. 8. Quantified $P_f$ fluctuation in different SNR with user interference.

three users under the normalized case are 55%, 25% and 12%, respectively, while under the non-normalized case, $P_d$ for the three users are 80%, 48% and 15%, respectively. This phenomenon demonstrates a clear enhancement in detection performance in the non-normalized case under the same conditions as the normalized case, attributed to the reduced impact of noise due to the higher relative signal power of the three users.

Fig. 8 manifests the quantified $P_f$ fluctuations between the two cases of user energy normalization and non-normalization across different SNR levels. The proposed-II method, shown in red, effectively mitigated false alarms ranging from -20 dB to 0 dB, whereas the proposed-I method, depicted in blue, exhibited a false alarm rate exceeding 50% in both the normalization case and the non-normalization case at 0 dB. Furthermore, as SNR increased, $P_f$ of the proposed-II method consistently remained below 10%. Thus, the proposed-II method consistently demonstrates lower fluctuation levels compared to the proposed-I method, highlighting its better robustness against interference.

Fig. 9 displays the performance comparison of throughput. Proposed-I-*A*, *B* and *C* all apply the single-orbit sensing approach, signifying that they only sense User 1, 2 and 3, respectively. It is evident that, with a fixed power allocation, the throughput of proposed-I-*A* markedly increases in comparison to proposed-I-*B* and *C*. This is due to the higher power of User 1 in comparison to User 2 and 3.

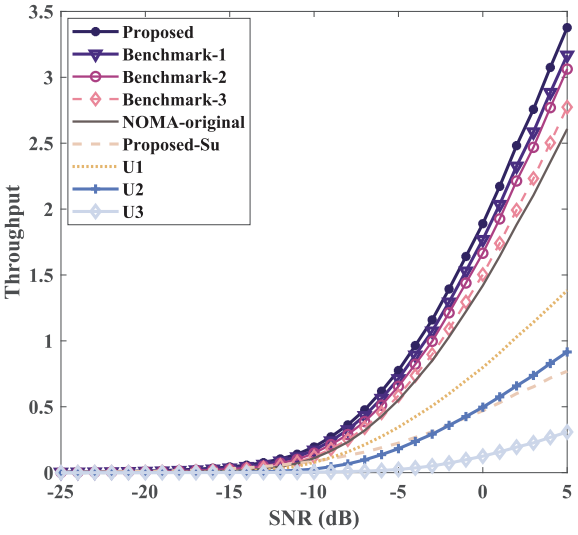


(a) Results with user energy normalization.

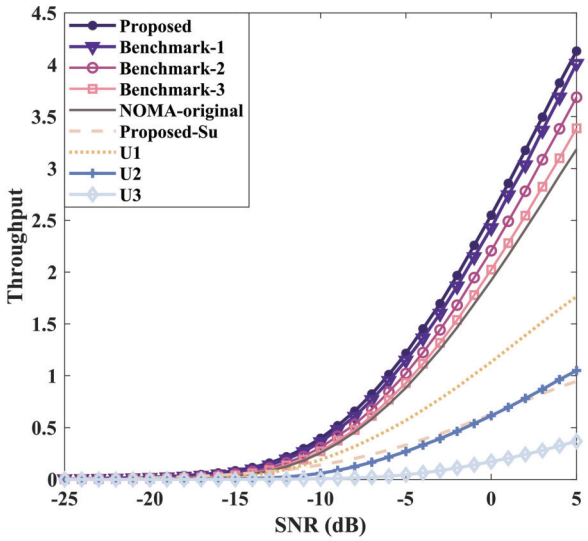


(b) Results without user energy normalization.

Fig. 9. System throughput of three-PUs uplink NOMA system under uncertainty PU transmitting probability with user interference.

Additionally, the proposed-II method results in significantly higher throughput than proposed-I-*B* and *C*. Based on this, the proposed-II method detects the resources in each orbit and selects the most powerful idle resource for transmission, to achieve more efficient sharing of spectrum resources. For the normalization case, this brings a 6.6% improvement at 5 dB SNR compared to the proposed-I-*A*. Compared to proposed-I-*B* and proposed-I-*C*, there is an improvement of about 10.5% and 21.6%, respectively. In summary, the performance of proposed-II method is outstanding, compared to the NOMA-benchmark, it can bring in 29.5% extra throughput gain at 5 dB for the normalization case. The similar trend of user and system throughput across normalized and non-normalized cases suggests that the proposed techniques are adaptable to diverse energy constraints, enhancing their practicality in real-world scenarios.

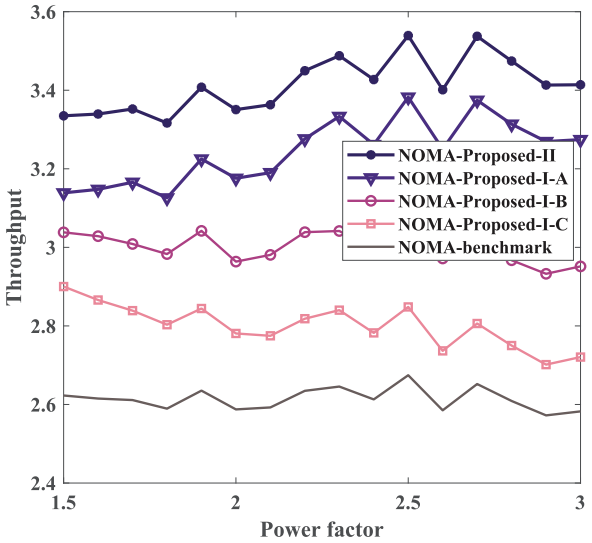


Fig. 10. System throughput of three-PUs uplink NOMA system with different power distribution under 5dB with user interference under user energy normalization.

Fig. 10 illustrates a comparison of system throughput performance when varying power allocation to PUs, with an SNR of 5 dB. The power factor, which determines the power multiplier between the three PUs, is denoted as '*a*'. For instance, a power factor of '*a*' indicates that the power of User 1 is '*a*' times that of User 2, and the power of User 2 is '*a*' times that of User 3. During its variation from 1.5 to 3, the values of throughput fluctuate due to the randomness of the signals transmitted by PUs. However, it is evident that the proposed-II method's system throughput consistently outperforms the proposed-I version's hard sensing, irrespective of these fluctuations. The proposed-II method shows a minimum improvement in throughput of around 4.3% and a maximum of about 6.1%, as the power changes, when compared to proposed-I-*A*. Correspondingly, the maximum throughput improvement is 15.6% and 25.4% as compared to proposed-I-*B* and *C*, respectively. Furthermore, proposed-II method has average 29.4% gain over NOMA-benchmark in terms of throughput.

Fig. 11 demonstrates a comparison of the system throughput in the four modes of the proposed-II method, as illustrated in Fig. 5. Mode 1 is a single-orbit random transmission, Mode 2 is a single-orbit optimal transmission, Mode 3 is a random aggregation, and Mode 4 is a greedy mode. Specifically, Mode 1 and 2 lack channel aggregation capability and use just one channel for transmission after sensing. In contrast, Mode 3 and 4 improve transmission performance through channel aggregation. The figure indicates that the greedy mode significantly enhances transmission the rate of SU by about 45% at 5 dB and improves the total system throughput by about 8.6% compared to the single-orbit random mode. In addition, the performance of both Mode 2 and Mode 3 are comparable, falling between that of Mode 1 and Mode 4.

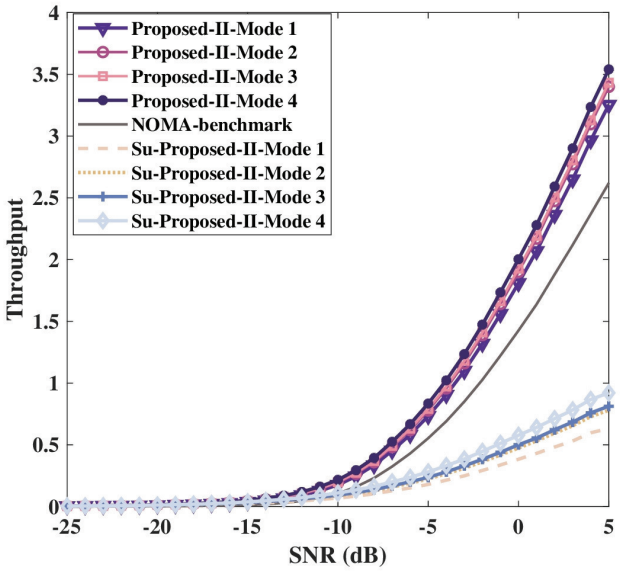


Fig. 11. System throughput of three-PUs uplink NOMA system with proposed 4 modes.

## V. Conclusion

This paper presents a spectrum sensing methodology for the multi-user uplink power-domain NOMA system in the presence of uncertain transmission pReferences and interference towards next-generation IoT networks. The objective is to optimize spectrum efficiency by leveraging both static and dynamic gains. The proposed method includes the development of a sensing criterion and workflow. In response to the variability in false-alarm probability, we regard non-fully occupied spectral holes resources as multiple orbits and enhanced the multi-user detection algorithm through the incorporation of orbit estimation, resulting in improved fault tolerance and mitigation of false-alarm probability fluctuations. The theoretical derivation of a closed-form solution for the relationship between the threshold and false-alarm probability has been achieved. The numerical results confirm the practicality and effectiveness of the comprehensive iteration of the proposed approach. Specifically, the proposed-II with orbit estimation has a larger throughput gain and more stable detection performance than the proposed-I with two typical fixed thresholds. In comparison to contemporary NOMA technologies, it ensures the detection probability while attaining an average system throughput gain of 30% at 5 dB.

## Acknowledgment

The authors would like to acknowledge the valuable support from the Xiaomi Fund of Young Scholar.

## References

[1] T. Xu et al., "Cyclic sensing: An orbital spectrum sensing method for uplink NOMA IoT systems," in *Proc. IEEE Int. Conf. Commun.*, Jun. 2024, pp. 373–378.

[2] F. Guo, F. R. Yu, H. Zhang, X. Li, H. Ji, and V. C. M. Leung, "Enabling massive IoT toward 6G: A comprehensive survey," *IEEE Internet Things J.*, vol. 8, no. 15, pp. 11891–11915, Aug. 2021.

[3] Q. Wu, X. Guan, and R. Zhang, "Intelligent reflecting surface-aided wireless energy and information transmission: An overview," *Proc. IEEE*, vol. 110, no. 1, pp. 150–170, Jan. 2022.

[4] C.-X. Wang et al., "On the road to 6G: Visions, requirements, key technologies, and testbeds," *IEEE Commun. Surveys Tuts.*, vol. 25, no. 2, pp. 905–974, 2nd Quart. 2023.

[5] X. Liu, H. Zhang, K. Sun, K. Long, and G. K. Karagiannidis, "AI-driven integration of sensing and communication in the 6G era," *IEEE Netw.*, vol. 38, no. 3, pp. 210–217, May 2024.

[6] *Framework and Overall Objectives of the Future Development of IMT for 2030 and Beyond*, ITU-R, Draft New Recommendation, Geneva, Switzerland, Jun. 2023.

[7] W. Feng et al., "Radio map-based cognitive satellite-UAV networks towards 6G on-demand coverage," *IEEE Trans. Cognit. Commun. Netw.*, vol. 10, no. 3, pp. 1075–1089, Jun. 2024.

[8] D. Li, "Ergodic capacity of intelligent reflecting surface-assisted communication systems with phase errors," *IEEE Commun. Lett.*, vol. 24, no. 8, pp. 1646–1650, Aug. 2020.

[9] Z. Gao et al., "Grant-free NOMA-OTFS paradigm: Enabling efficient ubiquitous access for LEO satellite Internet-of-Things," *IEEE Netw.*, vol. 37, no. 1, pp. 18–26, Jan. 2023.

[10] T. Janssen, A. Koppert, R. Berkvens, and M. Weyn, "A survey on IoT positioning leveraging LPWAN, GNSS, and LEO-PNT," *IEEE Internet Things J.*, vol. 10, no. 13, pp. 11135–11159, Jul. 2023.

[11] Y.-H. Chiang, H. Lin, and Y. Ji, "Information cofreshness-aware grant assignment and transmission scheduling for Internet of Things," *IEEE Internet Things J.*, vol. 8, no. 19, pp. 14435–14446, Oct. 2021.

[12] K. Banti, M. Louta, and P. Baziana, "Data quality in human-centric sensing-based next-generation IoT systems: A comprehensive survey of models, issues, and challenges," *IEEE Open J. Commun. Soc.*, vol. 4, pp. 2286–2317, 2023.

[13] M. Martalò, G. Pettorru, and L. Atzori, "A cross-layer survey on secure and low-latency communications in next-generation IoT," *IEEE Trans. Netw. Service Manage.*, vol. 21, no. 4, pp. 4669–4685, Aug. 2024.

[14] M. R. Nosouhi, K. Sood, M. Grobler, and R. Doss, "Towards spoofing resistant next generation IoT networks," *IEEE Trans. Inf. Forensics Security*, vol. 17, pp. 1669–1683, 2022.

[15] Q. Chen, W. Meng, T. Q. S. Quek, and S. Chen, "Multi-tier hybrid offloading for computation-aware IoT applications in civil aircraft-augmented SAGIN," *IEEE J. Sel. Areas Commun.*, vol. 41, no. 2, pp. 399–417, Feb. 2023.

[16] C. Shao, O. Muta, W. Wang, and W. Lee, "Toward ubiquitous connectivity via LoRaWAN: An overview of signal collision resolving solutions," *IEEE Internet Things Mag.*, vol. 4, no. 4, pp. 114–119, Dec. 2021.

[17] U. M. Malik, M. A. Javed, S. Zeadally, and S. U. Islam, "Energy-efficient fog computing for 6G-enabled massive IoT: Recent trends and future opportunities," *IEEE Internet Things J.*, vol. 9, no. 16, pp. 14572–14594, Aug. 2022.

[18] H. Zhang et al., "PPO-based PDACB traffic control scheme for massive IoV communications," *IEEE Trans. Intell. Transpoer. Syst.*, vol. 24, no. 1, pp. 1116–1125, Jan. 2023.

[19] T. Kim, J. Kwak, and J. P. Choi, "Satellite edge computing architecture and network slice scheduling for IoT support," *IEEE Internet Things J.*, vol. 9, no. 16, pp. 14938–14951, Aug. 2022.

[20] X. Yu and D. Li, "Phase shift compression for control signaling reduction in IRS-aided wireless systems: Global attention and lightweight design," *IEEE Trans. Wireless Commun.*, vol. 23, no. 8, pp. 8528–8541, Aug. 2024.

[21] X. Fang, W. Feng, T. Wei, Y. Chen, N. Ge, and C.-X. Wang, "5G embraces satellites for 6G ubiquitous IoT: Basic models for integrated satellite terrestrial networks," *IEEE Internet Things J.*, vol. 8, no. 18, pp. 14399–14417, Sep. 2021.

[22] Q. Wu et al., "Intelligent surfaces empowered wireless network: Recent advances and the road to 6G," *Proc. IEEE*, vol. 112, no. 7, pp. 724–763, Jul. 2024.

[23] X. Yang, M. Matthaiou, J. Yang, C.-K. Wen, F. Gao, and S. Jin, "Hardware-constrained millimeter-wave systems for 5G: Challenges, opportunities, and solutions," *IEEE Commun. Mag.*, vol. 57, no. 1, pp. 44–50, Jan. 2019.

[24] H. Xie, D. Li, and B. Gu, "Enhancing spectrum sensing via reconfigurable intelligent surfaces: Passive or active sensing and how many reflecting elements are needed?," *IEEE Trans. Wireless Commun.*, vol. 23, no. 10, pp. 14940–14955, Oct. 2024.

[25] Z. Wei et al., "Integrated sensing and communication signals toward 5G-A and 6G: A survey," *IEEE Internet Things J.*, vol. 10, no. 13, pp. 11068–11092, Jul. 2023.

[26] J. Wu, T. Xu, T. Zhou, X. Chen, N. Zhang, and H. Hu, "Feature-based spectrum sensing of NOMA system for cognitive IoT networks," *IEEE Internet Things J.*, vol. 10, no. 1, pp. 801–814, Jan. 2023.
[27] Z. Xu, Z. Sun, and L. Guo, "Throughput maximization of collaborative spectrum sensing under SSDF attacks," *IEEE Trans. Veh. Technol.*, vol. 70, no. 8, pp. 8378–8383, Aug. 2021.
[28] W. Yin and H. Chen, "Decision-driven time-adaptive spectrum sensing in cognitive radio networks," *IEEE Trans. Wireless Commun.*, vol. 19, no. 4, pp. 2756–2769, Apr. 2020.
[29] S. Surekha and M. Z. U. Rahman, "Spectrum sensing and allocation strategy for IoT devices using continuous-time Markov chain-based game theory model," *IEEE Sensors Lett.*, vol. 6, no. 4, pp. 1–4, Apr. 2022.
[30] J. Ye, X. Kang, Y.-C. Liang, and S. Sun, "A trust-centric privacy-preserving blockchain for dynamic spectrum management in IoT networks," *IEEE Internet Things J.*, vol. 9, no. 15, pp. 13263–13278, Aug. 2022.
[31] A. Huertas Celdrán, P. M. Sánchez Sánchez, C. Feng, G. Bovet, G. M. Pérez, and B. Stiller, "Privacy-preserving and syscall-based intrusion detection system for IoT spectrum sensors affected by data falsification attacks," *IEEE Internet Things J.*, vol. 10, no. 10, pp. 8408–8415, May 2023.
[32] A. M. Jaradat, M. I. Saglam, M. Kartal, and H. Arslan, "Dynamic-structure resource block allocation based scheduling for 5G systems," in *Proc. IEEE 95th Veh. Technol. Conf.*, Jun. 2022, pp. 1–5.
[33] Y. He, Y. Wang, Q. Lin, and J. Li, "Meta-hierarchical reinforcement learning (MHRL)-based dynamic resource allocation for dynamic vehicular networks," *IEEE Trans. Veh. Technol.*, vol. 71, no. 4, pp. 3495–3506, Apr. 2022.
[34] H. Zhang et al., "Energy efficient dynamic resource optimization in NOMA system," *IEEE Trans. Wireless Commun.*, vol. 17, no. 9, pp. 5671–5683, Sep. 2018.
[35] F. Ghanami, G. A. Hodtani, B. Vucetic, and M. Shirvanimoghaddam, "Performance analysis and optimization of NOMA with HARQ for short packet communications in massive IoT," *IEEE Internet Things J.*, vol. 8, no. 6, pp. 4736–4748, Mar. 2021.
[36] J. Wu, T. Xu, T. Zhou, X. Chen, H. Hu, and C. Wu, "Adaptive NOMA-based spectrum sensing for uplink IoT networks," *IEEE Trans. Cognit. Commun. Netw.*, vol. 10, no. 1, pp. 138–149, Feb. 2024.
[37] Z. Wang, L. Xiong, X. Liu, and M. Peng, "Successive interference cancellation for communication and radar coexistence," in *Proc. IEEE 95th Veh. Technol. Conf.(VTC-Spring)*, Jun. 2022, pp. 1–5.
[38] B. Sri Pavan and V. P. Harigovindan, "Power-optimized NOMA with TXOP tuning-based channel access scheme for IEEE 802.11ah dense IoT networks," *IEEE Netw. Lett.*, vol. 4, no. 4, pp. 179–183, Dec. 2022.
[39] M. Asif, A. Ihsan, W. U. Khan, A. Ranjha, S. Zhang, and S. X. Wu, "Energy-efficient beamforming and resource optimization for AmBSC-assisted cooperative NOMA IoT networks," *IEEE Internet Things J.*, vol. 10, no. 14, pp. 12434–12448, Jul. 2023.
[40] D. Sarkar, S. S. Yadav, V. Pal, Yogita, and N. Kumar, "Intelligent reflecting surface aided NOMA-HARQ based IoT framework for future wireless networks," *IEEE Trans. Veh. Technol.*, vol. 72, no. 5, pp. 6268–6280, May 2023.
[41] C. Wang, R. Zhang, J. Tan, and B. Jiao, "Hybrid NOMA user grouping for short packet communications in IoT network with different types of devices," in *Proc. IEEE Int. Conf. Commun. Workshops (ICC Workshops)*, Seoul, South Korea, May 2022, pp. 228–234.
[42] Z. Liu, X. Liu, V. C. M. Leung, and T. S. Durrani, "Energy-efficient resource allocation for dual-NOMA-UAV assisted Internet of Things," *IEEE Trans. Veh. Technol.*, vol. 72, no. 3, pp. 3532–3543, Mar. 2023.
[43] T.-H. Vu, T.-V. Nguyen, and S. Kim, "Cooperative NOMA-enabled SWIPT IoT networks with imperfect SIC: Performance analysis and deep learning evaluation," *IEEE Internet Things J.*, vol. 9, no. 3, pp. 2253–2266, Feb. 2022.
[44] D. A. Tubiana, J. Farhat, G. Brante, and R. D. Souza, "Q-learning NOMA random access for IoT-satellite terrestrial relay networks," *IEEE Wireless Commun. Lett.*, vol. 11, no. 8, pp. 1619–1623, Aug. 2022.
[45] T. Park, G. Lee, W. Saad, and M. Bennis, "Sum rate and reliability analysis for power-domain nonorthogonal multiple access (PD-NOMA)," *IEEE Internet Things J.*, vol. 8, no. 12, pp. 10160–10169, Jun. 2021.
[46] A. Yadav, C. Quan, P. K. Varshney, and H. V. Poor, "On performance comparison of multi-antenna HD-NOMA, SCMA, and PD-NOMA schemes," *IEEE Wireless Commun. Lett.*, vol. 10, no. 4, pp. 715–719, Apr. 2021.
[47] M. Wen, S. Lin, K. J. Kim, and F. Ji, "Cyclic delay diversity with index modulation for green Internet of Things," *IEEE Trans. Green Commun. Netw.*, vol. 5, no. 2, pp. 600–610, Jun. 2021.
[48] J. Xu, S. Zhu, and Z. Gao, "Partial-differential distributed cyclic delay diversity for nonregenerative two-way relaying system," *IEEE Signal Process. Lett.*, vol. 16, no. 7, pp. 596–599, Jul. 2009.
[49] Z. Fang, J. Hu, Y. Lu, and W. Ni, "Three-user cooperative NOMA transmission," *IEEE Wireless Commun. Lett.*, vol. 9, no. 4, pp. 465–469, Apr. 2020.
[50] R. Ramesh, S. Gurugopinath, and S. Muhaidat, "Three-user cooperative dual-stage non-orthogonal multiple access for power line communications," *IEEE Open J. Commun. Soc.*, vol. 4, pp. 184–196, 2023.
[51] F. Fang, Z. Ding, W. Liang, and H. Zhang, "Optimal energy efficient power allocation with user fairness for uplink MC-NOMA systems," *IEEE Wireless Commun. Lett.*, vol. 8, no. 4, pp. 1133–1136, Aug. 2019.
[52] S. Hu, H. Huang, G. Gui, and H. Sari, "An analysis of the power imbalance on the uplink of power-domain NOMA," in *Proc. IEEE 96th Veh. Technol. Conf.(VTC-Fall)*, Sep. 2022, pp. 1–5.

**Tianheng Xu** (Member, IEEE) received the Ph.D. degree from Shanghai Institute of Microsystem and Information Technology, Chinese Academy of Sciences, Shanghai, China, in 2016. He is currently a Full Professor and the Deputy Director of the Intelligent Information and Communication Research Center, Shanghai Advanced Research Institute, Chinese Academy of Sciences. His research interests include 5G/6G wireless communications, ubiquitous cognition and intelligent spectrum sensing technology, and multimodal signal processing and heterogeneous system interaction technologies. He received the President Scholarship of Chinese Academy of Sciences (First Grade) in 2014, the Outstanding Ph.D. Graduates Award of Shanghai in 2016, the Best Paper Award at the IEEE GLOBECOM 2016, and the Springer MONAMI 2021; the First Prize and Second Prize of Technological Invention Awards from China Institute of Communication in 2019 and 2024, respectively; and the First Prize of Shanghai Technological Invention Awards in 2020 and 2022, respectively.

**Yinjun Xu** (Member, IEEE) received the B.S. degree from Northwestern Polytechnical University, Xi'an, China, in 2021, and the M.S. degree from Shanghai Advanced Research Institute, Chinese Academy of Sciences, Shanghai, China, in 2024. His research interests include key technologies of spectrum sensing, non-terrestrial communications, and non-orthogonal multiple access for next generation wireless communication.

**Jingyi Wu** received the B.S. degree from Zhejiang University, Hangzhou, China, in 2020, and the M.S. degree from Shanghai Advanced Research Institute, Chinese Academy of Sciences, Shanghai, China, in 2023. Her research interests include key technologies of spectrum sensing and non-orthogonal multiple access for next generation wireless communication.

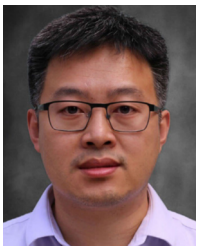

**Haijun Zhang** (Fellow, IEEE) was a Post-Doctoral Research Fellow with the Department of Electrical and Computer Engineering, The University of British Columbia (UBC), Canada. He is currently a Full Professor with the University of Science and Technology Beijing, China. He received the IEEE CSIM Technical Committee Best Journal Paper Award in 2018, the IEEE ComSoc Young Author Best Paper Award in 2017, and the IEEE ComSoc Asia–Pacific Best Young Researcher Award in 2019. He serves/served as the Track Co-Chair for VTC Fall 2022 and WCNC 2020/2021, the Symposium Chair for GLOBECOM'19, the TPC Co-Chair for INFOCOM 2018 Workshop on Integrating Edge Computing, Caching, and Offloading in Next Generation Networks, and the General Co-Chair for GameNets'16. He serves/served as an Editor for IEEE TRANSACTIONS ON COMMUNICATIONS and IEEE TRANSACTIONS ON NETWORK SCIENCE AND ENGINEERING. He is a Distinguished Lecturer of IEEE.

**Ting Zhou** (Member, IEEE) received the B.S. and M.S. degrees from the Department of Electronic Engineering, Tsinghua University, in 2004 and 2006, respectively, and the Ph.D. degree from Shanghai Institute of Microsystem and Information Technology, Chinese Academy of Sciences, in 2011. She is currently a Full Professor and the Deputy Director of the School of Microelectronics, Shanghai University. Her research interests include wireless resource management and mobility management, intelligent networking of heterogeneous wireless networks, and 6G mobile systems. She was awarded "Shanghai Young Scientific and Technological Talents" in 2022 and led to won the First Prize of Shanghai Science and Technology Awards in 2020 and 2022, respectively.

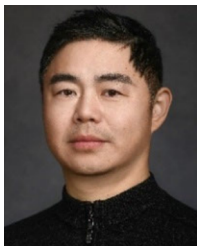

**Honglin Hu** (Senior Member, IEEE) received the Ph.D. degree in communications and information system from the University of Science and Technology of China, Langfang, China, in 2004. He was with the Future Radio, Siemens AG Communications, Hamburg, Germany. From 2015 to 2018, he was a Finland Distinguished Professor with the VTT Technical Research Centre of Finland, Oulu, Finland. Since 2009, he has been a Full Professor with Shanghai Institute of Microsystem and Information Technology, Chinese Academy of Sciences, Shanghai, China. Since 2013, he has been an Adjunct Professor with ShanghaiTech University, Shanghai, and the Vice Director of Shanghai Research Center for Wireless Communications, Shanghai. He is currently a Full Professor and the Director of the Intelligent Information and Communication Research Center, Shanghai Advanced Research Institute, Chinese Academy of Sciences. He was a recipient of the 2016 IEEE Jack Neubauer Memorial Award (the Best Paper Award of the IEEE TRANSACTIONS ON VEHICULAR TECHNOLOGY) and the Best Paper Award from the IEEE GLOBECOM 2016. He was the Vice Chair of the IEEE Shanghai Section. He was a Leading Guest Editor of IEEE WIRELESS COMMUNICATIONS special issue on Mobile Converged Networks and *IEEE Communications Magazine* special issue on Software Defined Wireless Networks (Part I and Part II).

**Victor C. M. Leung** (Life Fellow, IEEE) is currently the Dean of the Artificial Intelligence Research Institute, Shenzhen MSU-BIT University, Shenzhen, China, a Distinguished Professor of computer science and software engineering with Shenzhen University, Shenzhen, and a Professor Emeritus with The University of British Columbia (UBC), Vancouver, Canada. Before he retired from UBC, in 2018, he was a Professor of electrical and computer engineering and the Holder of the TELUS Mobility Research Chair. He has co-authored more than 1300 journals/conference papers and book chapters. His research interests include wireless networks and mobile systems. He is a fellow of the Royal Society of Canada, Canadian Academy of Engineering, and the Engineering Institute of Canada. He received the IEEE Vancouver Section Centennial Award, the 2011 UBC Killam Research Prize, the 2017 Canadian Award for Telecommunications Research, and the 2018 IEEE TCGCC Distinguished Technical Achievement Recognition Award. He co-authored papers that won the 2017 IEEE ComSoc Fred W. Ellersick Prize, the 2017 IEEE Systems Journal Best Paper Award, the 2018 IEEE CSIM Best Journal Paper Award, and the 2019 IEEE TCGCC Best Journal Paper Award. He is named in the current Clarivate Analytics List of "Highly Cited Researchers." He is serving on the editorial boards for IEEE TRANSACTIONS ON GREEN COMMUNICATIONS AND NETWORKING, IEEE TRANSACTIONS ON COMPUTING, IEEE ACCESS, and IEEE NETWORK, and several other journals.